

Note on the electromagnetic radius of proton

M. Ridwan and T. Mart

*Departemen Fisika, FMIPA, Universitas Indonesia, Depok 16424, Indonesia
terry.mart@sci.ui.ac.id*

Received Day Month Year

Revised Day Month Year

We have analyzed the proton form factor data by using a number of phenomenological parameterizations (models) and extracting the proton electric and magnetic radii. To this end we performed a global fit to all available form factor data, with the virtual photon momentum squared Q^2 from 0.0002 to nearly 10 GeV² for electric form factor and from 0.015 to 31 GeV² for magnetic one. Special attention was given to the small structure shown by the form factor data near $Q^2 = 0.2$ GeV². It was found that different models yield different structures with different numbers of minimum at this kinematics. Since the slope of form factor in the limit of $Q^2 \rightarrow 0$ is influenced by this structure, the extracted proton radii are consequently different for different models. Our finding recommends that future experiments should focus on this kinematics instead of low Q^2 . Experimental data with accuracies comparable to those of the latest data at low Q^2 would clearly help to clarify the effect of this structure on the proton charge radius. Interestingly, most of the extracted proton charge radii were found to be closer to the value obtained from the muonic hydrogen atom spectroscopy.

Keywords: Proton; neutron; form factors; charge radius; magnetic radius.

PACS numbers: 13.40.Gp, 13.85.Dz, 14.20.Dh

1. Introduction

Since the work of Nobel laureate Robert Hofstadter in fifties,¹ the elastic electron-proton scattering has become a standard tool to determine the radius of proton. It was found that the structure of the proton can be best explained by using a dipole form factor with a cut-off $\Lambda^2 = 0.71$ GeV² and, surprisingly, in a wide range of virtual photon momentum squared Q^2 . Decades after that, however, it was found that this parameterization cannot explain newer data produced by modern electron accelerator laboratories with unprecedented precise particle detectors. Nevertheless, the dipole form factor $G_{SD} = (1 + Q^2/0.71 \text{ GeV}^2)^{-2}$ is still used in textbooks and state-of-the-art analyses as a standard one and known as the standard dipole form factor.

For present purpose, it is important to mention a number of modern electron-proton scattering experiments performed in the last decade. The first precise experiment² was done in MAMI at Mainz in 2010. From this experiment thousands

cross section data points were extracted and fitted to obtain the electric $G_{E,p}$ and magnetic $G_{M,p}$ form factors of proton. The proton charge radius $r_E = 0.879 \pm 0.008$ fm and the magnetic one $r_M = 0.777 \pm 0.017$ fm were obtained from these data. This experiment was followed by another one, using the same spectrometer but different technique designed to reach very small Q^2 , i.e., the initial-state radiation (ISR). By using the ISR technique, the cross section data were obtained with Q^2 from 0.001 to 0.004 GeV². The first extracted radius³ was $r_E = 0.810 \pm 0.082$ fm. Three years later, by improving the calculation and reinterpretation of these data, the experimentalists in Mainz obtained⁴ a radius of $r_E = 0.878 \pm 0.033$ fm.

By measuring the polarization transfer in electron-proton elastic scattering the experimentalists in Hall A of Jefferson Lab were able to determine the ratio $\mu_p G_{E,p}/G_{M,p}$ with high precision. A global fit⁵ to the combination of these data with previous available data yields a proton radius of $r_E = 0.875 \pm 0.010$ fm. Note that, except the previous Mainz ISR report, all results from elastic electron-proton scattering experiments are consistent with the value obtained from the Mainz-2010 one.²

Very recently, the PRad collaboration⁶ performed another precise elastic electron-proton scattering experiment at Jefferson Lab. To reach significantly low Q^2 values, the PRad experiment used two-dimensional high-resolution electromagnetic calorimeter, instead of a conventional magnetic spectrometer. By exploiting this calorimeter, smaller scattering angles could be covered and, as a consequence, Q^2 range from 0.0002 to 0.0600 GeV² could be reached. The extracted proton radius was found to be $r_E = 0.831 \pm 0.014$ fm, which is surprisingly inconsistent with the values obtained from the conventional elastic electron-proton scattering.

On the other hand, the electromagnetic radius of proton can be also determined by means of the spectroscopy of electronic and muonic hydrogen atoms. This is possible since the effect of proton's finite size in hydrogen atom on hydrogen energy⁷ is proportional to the proton's squared radius $\langle r_{E,p}^2 \rangle \equiv r_E^2$. The first modern muonic hydrogen spectroscopic experiment to this end was performed at Paul Scherrer Institute by measuring the frequency of transition between $2S_{1/2}^{F=1}$ and $2P_{1/2}^{F=2}$ states.⁸ The obtained proton charge radius is 0.84184 ± 0.00067 fm, significantly smaller than that obtained from electron-proton scattering experiments. This result surprised the community, because the theoretical calculation used to extract the radius is based only on quantum electrodynamics and, therefore, has much less uncertainties.

The publication of the first proton radius extraction from muonic hydrogen atom in 2010 was followed by the publications of four similar experiments, but using conventional electronic hydrogen. By measuring the $2S - 4P$ transition in electronic hydrogen atom, the experimentalists in Garching⁹ were able to determine the radius to be $r_E = 0.8335 \pm 0.0095$ fm, which is consistent with the radius obtained from muonic hydrogen atom. Another similar experiment in Paris¹⁰ measured the $1S - 3S$ two-photon transition and reported a radius of $r_E = 0.877 \pm 0.013$ fm, consistent with that obtained from electron-proton scattering. Two other similar experiments found the proton radius to be $r_E = 0.833 \pm 0.010$ fm¹¹ and $r_E = 0.8482 \pm 0.0038$

fm,¹² which are closer to the result of muonic hydrogen atom.

The large differences among the extracted proton radii obtained by different experiments sparked the so called proton radius puzzle in the community. Actually, before this puzzle attracted the attention of the community, there had been two other puzzles, i.e., the proton mass puzzle and the proton spin crisis.

There have been considerable efforts devoted to resolve the proton radius puzzle, spanning from field theory to extra dimension. Since it is not our intention to discuss this puzzle, along with the proposed solutions, in detail, we refer the interested reader to a recent review by Gao and Vanderhaeghen¹³ on this topic for a more comprehensive information. Nevertheless, it is important to note that this review concludes that the proton charge radius puzzle has not been resolved yet. More experimental results from electron-proton scattering as well as from hydrogen spectroscopy are required to fully resolve this puzzle. A similar conclusion can be also drawn from the present work discussed in this note.

In this note, we would like to raise the issue of high Q^2 proton form factor data and their effect on the extraction of the proton radius. We observe that most of experimental and theoretical analyses are focused on low or even very low Q^2 region. Of course, this is understandable, since by definition the radius of proton is determined by the slope of its form factor at $Q^2 = 0$. Thus, most experimental and theoretical investigations to this end are competing to reach the lowest possible Q^2 . On the other hand, it is also clear that in the limit of $Q^2 \rightarrow 0$ the slope of form factor would also be influenced by the higher Q^2 data, if we performed a global fit (fit to all available Q^2). Interestingly, in the case of proton electric form factor $G_{E,p}$ there is a minuscule structure at $Q^2 \approx 0.2 \text{ GeV}^2$, which is almost invisible if we just plot the form factor data as a function of Q^2 . This structure was discussed two decades ago by Friedrich and Walcher and interpreted as a contribution of pion cloud.¹⁴ In this note we found that in order to clearly see this structure, we should present the form factors in term of the standard dipole one, G_{SD} . Similar structure is also observed in the magnetic form factor of proton $G_{M,p}$.

A global fit to proton form factor data has been also discussed in the literature, e.g., by Arrington *et al.*⁵ and Atac *et al.*¹⁵. However, comparing with the analyses of the low Q^2 data, they are relatively seldom. Furthermore, these analyses usually did not pay a special attention on the structure existing at $Q^2 \approx 0.2 \text{ GeV}^2$. In the present note, we simultaneously focus on this structure and extract the proton radii from a global fit by using several form factor models, including the Friedrich-Walcher and Arrington ones. Similar studies focusing on the dependence of the extracted proton radius on the form factor models and Q^2 cut-off can be found, e.g., in Refs.^{16–27}.

The organization of this note is as follows. In Sec. 2 we revisit the formalism required for extracting the electromagnetic radius of proton. We present several form factor parameterizations (models), which include the dipole, double-dipole, Friedrich-Walcher, and Arrington ones. We also derive the corresponding error bar

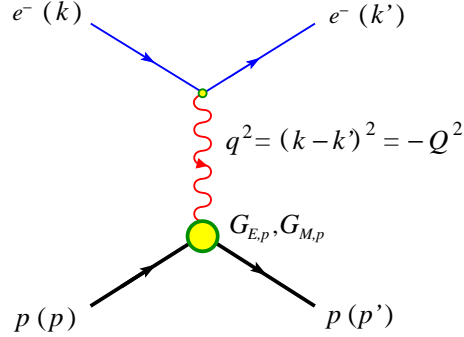


Fig. 1. Kinematics of the electron-proton elastic scattering. The four-momenta of the initial and final electrons are defined as $k^\mu = (E, \mathbf{k})$ and $k'^\mu = (E', \mathbf{k}')$, respectively.

formulas required for our present analysis. In Sec. 3 we present the result of our analysis. We start with reanalyzing the PRad data and then we continue by including higher Q^2 data in our analysis. The obtained proton charge and magnetic radii in the present work will be discussed in this section. We close this note by presenting the summary and conclusion in Sec. 4.

2. Formalism

2.1. Elastic Electron-Proton Scattering

Conventionally, the elastic electron-proton scattering process is depicted in Fig. 1, where the one-photon exchange process is assumed. The kinematical variable required in the following discussion is only the opposite of the virtual photon momentum squared $Q^2 = -q^2$. The cross section is given in most standard textbooks. It is usually expressed in terms of the electric and magnetization (Sachs) form factors G_E and G_M , which depend solely on Q^2 , i.e.,

$$\left(\frac{d\sigma}{d\Omega}\right)_N = \left(\frac{d\sigma}{d\Omega}\right)_{\text{Mott}} \frac{1}{1 + \tau} \left[G_E^2(Q^2) + \frac{\tau}{\epsilon} G_M^2(Q^2) \right], \quad (1)$$

where $\tau = Q^2/4M^2$, M is the proton mass, and the Mott cross section is given by

$$\left(\frac{d\sigma}{d\Omega}\right)_{\text{Mott}} = \frac{\alpha^2 \cos^2(\theta/2)}{4E^2 \sin^4(\theta/2)} \frac{E'}{E}, \quad (2)$$

with E and E' the initial and final electron energies, respectively, defined in Fig. 1, whereas the virtual photon polarization reads

$$\epsilon = \left[1 + 2(1 + \tau) \tan^2 \frac{\theta}{2} \right]^{-1}. \quad (3)$$

For completeness, we have also to mention that θ is the electron scattering angle and in the limit of $Q^2 \rightarrow 0$ the form factors are normalized to

$$G_E(0) = 1, \quad G_M(0) = 1 + \kappa = \mu \quad \text{or} \quad G_M(0)/\mu = 1, \quad (4)$$

where μ is the proton magnetic moment in the unit of nuclear magneton.

In the non-relativistic view it is common to interpret the form factors G_E and G_M as the Fourier transforms of charge and magnetization distributions inside the proton

$$G_{E,M}(Q^2) = \int \rho_{E,M}(\mathbf{r}) e^{i\mathbf{q}\cdot\mathbf{r}} d\mathbf{r} . \quad (5)$$

However, it is well known that this is not true in the relativistic case, where the relativistic wave functions are frame dependent and, therefore, the interpretation is only valid in the case of Breit frame. There have been solutions proposed to solve this problem. For instance, see Refs.^{13,28}. Nevertheless, for the operational definition of the form factor slope at photon point, we can Taylor expand the form factors as¹³

$$G_{E,M}(Q^2) = 1 - \frac{1}{6} \langle r_{E,M}^2 \rangle Q^2 + \frac{1}{120} \langle r_{E,M}^4 \rangle Q^4 - \dots , \quad (6)$$

from which we can calculate the corresponding root mean square (rms) radius as

$$r_{E,M} = \sqrt{\langle r_{E,M}^2 \rangle} = \left[-6 \frac{dG_{E,M}(Q^2)}{dQ^2} \Big|_{Q^2=0} \right]^{1/2} . \quad (7)$$

It is important to emphasize here that the squared radius defined by Eq. (7) is, up to the factor of -6 , nothing but the slope of the form factor at $Q^2 = 0$. Thus, although the recent and modern data bring us much closer to this photon point, the determination of radius by using this method is merely an estimate, which is strongly influenced by the data at both small and large Q^2 . The latter is the main interest in this note and will be shown in the next section, when we discuss the result of our analysis.

2.2. Phenomenological Fits of the Form Factors

For decades the standard dipole form factor

$$G_{\text{SD}}(Q^2) = \left(1 + \frac{Q^2}{0.71 \text{ GeV}^2} \right)^{-2} = \left[1 + \frac{Q^2}{(0.84 \text{ GeV})^2} \right]^{-2} \quad (8)$$

has been used to fit the available experimental data, from very low to very high Q^2 . The impressive agreement between Eq. (8) and experimental data has led to the question whether the special parameter 0.71 GeV^2 has a physical meaning related to the structure of the proton. Unfortunately, there is none.¹⁴ Moreover, it was soon realized that the Q^2 distribution of experimental data are not smooth; they form a structure at $Q^2 \approx 0.2 \text{ GeV}^2$, which is clearly not reproducible by using Eq. (8). Nevertheless, it is always interesting to use the dipole form factor

$$G_{\text{D}}(Q^2) = \left(1 + \frac{Q^2}{\Lambda^2} \right)^{-2} , \quad (9)$$

in the study of general baryon form factors and to fit the parameter Λ , since it is the simplest possible form factor to this end. Furthermore, we are also curious to investigate the limit of dipole form factor in view of the recent available experimental data in the low Q^2 region. Note that by using Eq. (7) to the dipole parameterization given by Eq. (9) we obtain the rms radius of

$$r_D \equiv \sqrt{\langle r_D^2 \rangle} = \frac{\sqrt{12}}{\Lambda}, \quad (10)$$

with error given by

$$\Delta r_D = r_D \frac{\Delta \Lambda}{\Lambda}. \quad (11)$$

Note that using the form factor parameter given by the standard dipole of Eq. (8), $\Lambda = 0.84 \text{ GeV} = 4.26 \text{ fm}^{-1}$, the corresponding radius according to Eq. (10) is 0.81 fm, much smaller than that obtained from present experiments using elastic electron-proton scattering.

A modification to the dipole form factor, Eq. (9), is known as the double dipole (DD) one. The DD form factor is certainly more flexible than the dipole one due to the addition of two new parameters a_0 and a_2 , whereas $a_1 \equiv \Lambda$, i.e.,

$$G_{DD}(Q^2, a_0, a_1, a_2) = a_0 \left(1 + \frac{Q^2}{a_1}\right)^{-2} + (1 - a_0) \left(1 + \frac{Q^2}{a_2}\right)^{-2}. \quad (12)$$

Note that G_{DD} is properly normalized at photon point, i.e., $G_{DD}(0, a_0, a_1, a_2) = 1$. It is straightforward to calculate the rms radius given by Eq. (12). The obtained radius reads

$$r_{DD} = \sqrt{12} \left(\frac{a_0}{a_1} + \frac{1 - a_0}{a_2} \right)^{1/2}, \quad (13)$$

with the corresponding error

$$\Delta r_{DD} = \frac{6}{r} \left\{ (\Delta a_0)^2 \left(\frac{1}{a_1} - \frac{1}{a_2} \right)^2 + (\Delta a_1)^2 \left(\frac{a_0}{a_1^2} \right)^2 + (\Delta a_2)^2 \left(\frac{1 - a_0}{a_2^2} \right)^2 \right\}^{1/2}. \quad (14)$$

To account for the small structure at $Q^2 \approx 0.2 \text{ GeV}^2$ Friedrich and Walcher (FW) added a non-smooth term G_{ns} to the DD form factor given by Eq. (12), with

$$G_{ns}(Q^2, Q_b, \sigma_b) = \exp \left\{ -\frac{1}{2} \left(\frac{Q - Q_b}{\sigma_b} \right)^2 \right\} + \exp \left\{ -\frac{1}{2} \left(\frac{Q + Q_b}{\sigma_b} \right)^2 \right\}. \quad (15)$$

Thus, the complete expression for the FW form factor is¹⁴

$$G_{FW}(Q^2, a_0, a_1, a_2, Q_b, \sigma_b) = G_{DD}(Q^2, a_0, a_1, a_2) + a_b Q^2 G_{ns}(Q^2, Q_b, \sigma_b). \quad (16)$$

It is obvious that the corresponding expressions of radius and its error can be obtained from Eqs. (13) and (14) with the addition of the non-smooth contribution.

Explicitly, they read

$$r_{\text{FW}} = \sqrt{12} \left\{ \frac{a_0}{a_1} + \frac{1-a_0}{a_2} - a_b \exp\left(-\frac{Q_b^2}{2\sigma_b^2}\right) \right\}^{1/2}, \quad (17)$$

and

$$\begin{aligned} \Delta r_{\text{FW}} = \frac{6}{r} & \left[(\Delta a_0)^2 \left(\frac{1}{a_1} - \frac{1}{a_2} \right)^2 + (\Delta a_1)^2 \left(\frac{a_0}{a_1^2} \right)^2 + (\Delta a_2)^2 \left(\frac{1-a_0}{a_2^2} \right)^2 \right. \\ & \left. + \left\{ (\Delta a_b)^2 + (\Delta Q_b)^2 \frac{a_b^2 Q_b^2}{\sigma_b^4} + (\Delta \sigma_b)^2 \frac{a_b^2 Q_b^4}{\sigma_b^6} \right\} \exp\left(-\frac{Q_b^2}{\sigma_b^2}\right) \right]^{1/2}. \quad (18) \end{aligned}$$

The last model investigated in this work is obtained from the Arrington *et al.* ansatz.⁵ In this ansatz the form factor is expanded in a polynomial form, i.e.,

$$G_{\text{Arr}} = \frac{1 + \sum_{i=1}^n a_i \tau^i}{1 + \sum_{i=1}^{n+2} b_i \tau^i}, \quad (19)$$

with $\tau = Q^2/4M^2$ and M is the proton mass. Although the summation in Eq. (19) could be performed up to infinity, Arrington *et al.* limited it to $n = 3$. Thus, Eq. (19) reduces to

$$G_{\text{Arr}} = \frac{1 + a_1 \tau + a_2 \tau^2 + a_3 \tau^3}{1 + b_1 \tau + b_2 \tau^2 + b_3 \tau^3 + b_4 \tau^4 + b_5 \tau^5}. \quad (20)$$

Since only parameters a_1 and b_1 are proportional to the Q^2 , only these parameters survive in the limit of photon point. As a consequence, the corresponding radius and error are given only in terms of a_1 and b_1 . Explicitly, they are given by

$$r_{\text{Arr}} = \sqrt{\frac{3}{2}} \frac{(b_1 - a_1)^{1/2}}{M}, \quad (21)$$

with the corresponding error

$$\Delta r_{\text{Arr}} = \frac{3}{4M^2 r_{\text{Arr}}} \{(\Delta a_1)^2 + (\Delta b_1)^2\}^{1/2}. \quad (22)$$

3. Results and Discussion

The minimization process in this work was performed by using the MINUIT code.²⁹ We combined the SIMPLEX and MIGRAD minimizers in the minimization process until the MIGRAD reaches the convergence. All errors reported here are only those obtained from the MINUIT output.

3.1. Revisiting PRad Data

As stated in the Introduction, the latest measurement by the PRad collaboration⁶ is very interesting to analyze, since the corresponding data yield a smaller proton radius, compared to those obtained by different collaborations. Furthermore, the extracted radius is consistent with the muonic-hydrogen atom experiment.⁸ It is

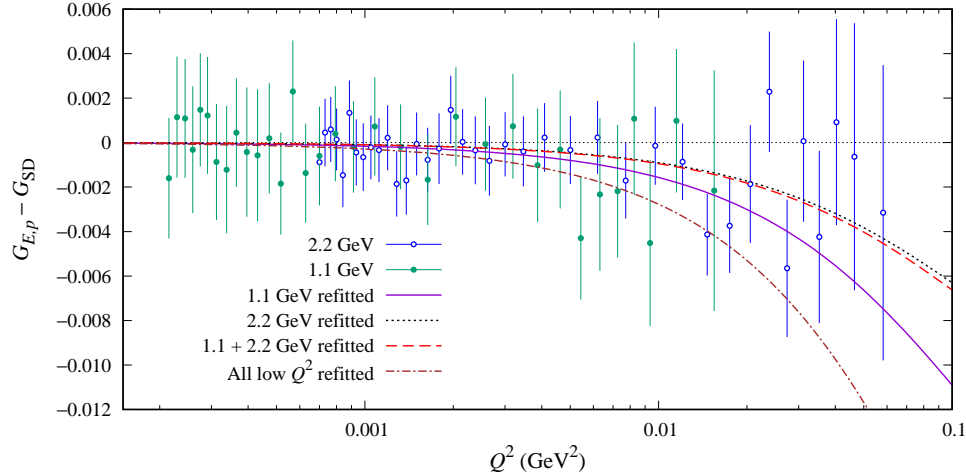


Fig. 2. The relative electric form factor of proton to the standard dipole one, $G_{E,p} - G_{SD}$, measured by the PRad collaboration⁶ with electron beam energies $E = 1.1$ (closed circles) and 2.2 (open circles) GeV, compared with the results of fitting to different sets of experimental data.

notoriously known that the data points with very small Q^2 have the form factors very close to one and, therefore, difficult to distinguish. To overcome this problem, in Fig. 2 we plot the relative electric form factor of proton to the standard dipole one, $G_{E,p} - G_{SD}$. As will be explained in the next figures, for this purpose the use of $G_{E,p} - G_{SD}$ is superior than that of $G_{E,p}/G_{SD}$ or $G_{E,p}$ itself. Furthermore, for the sake of brevity, let us define $\Delta \equiv G_{E,p} - G_{SD}$.

At first glance we may say that both the 1.1 and 2.2 GeV PRad data are randomly scattered around the standard dipole G_{SD} curve, i. e., around $\Delta = 0$. Only for $Q^2 \geq 0.005$ GeV² more data start to deviate from the standard dipole parameterization with negative Δ , albeit with relatively large error bars.

In their report, PRad collaboration used the parameterization similar to the Arrington model, i. e., Eq. (19) with $n = 1$ both in the numerator and denominator. Furthermore, a more complicated treatment was also used in order to achieve an optimal χ^2 . In this analysis, we will only use the dipole form factor, since it is simpler and more under-control. The result of fitting this dipole form factor to different data sets is shown in Fig. 2, where for comparison we also show the result of fitting to all available low Q^2 data that include older experiments.

It is apparent from Fig. 2 that the 1.1 GeV data set yields slightly larger slope, i. e., larger radius and smaller Λ . The more scattered data points of the 2.2 GeV data set, especially for $Q^2 \geq 0.005$ GeV², tend to decrease the extracted radius. Thus, different data sets from the same experiment can produce different proton radii. Furthermore, since fitting both 1.1 and 2.2 GeV data sets simultaneously yields almost similar result to fitting to 2.2 GeV data set (compare the dotted and

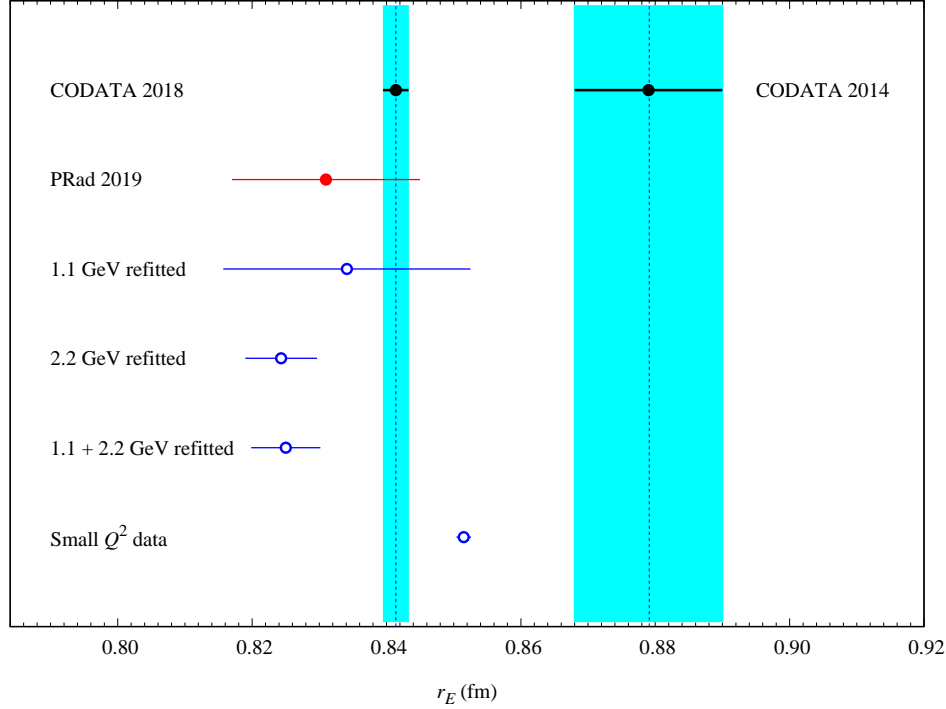


Fig. 3. The extracted radii of proton obtained from fitting to different experimental databases shown in Fig. 2, compared with those reported by CODATA 2014³⁰ and CODATA 2018.³¹

dashed curves in Fig. 2), this indicates that the data with higher Q^2 values are more decisive for determination of the proton radius. This is obvious, since the slope is strongly dependent on the higher Q^2 behavior of form factor.

The extracted radii obtained from different data sets given in Fig. 2 are shown in Fig. 3, where we also show the original value extracted by the PRad collaboration and the recommended values from CODATA 2014³⁰ and CODATA 2018.³¹ As originally reported by the PRad collaboration,⁶ they obtained the radius consistent with the later CODATA value. As shown in Fig. 3, in spite of the use of different parameterization, within the obtained error bars all values extracted in the present work by using different PRad data sets are consistent with the original one. The most consistent radius is obtained from fitting the 1.1 GeV data. The use of 2.2 GeV data (individually and simultaneously) yields smaller values and error bars. This is in line with the previous finding in the discussion of Fig. 2. Therefore, we confirm the finding of the PRad collaboration that their data lead to smaller radius, closer to the value obtained from the muonic hydrogen atom spectroscopy.

We also note that fitting to all other data with small Q^2 , i.e., up to 0.06 GeV², results in a larger radius. Nevertheless, it is still closer to the value from muonic

hydrogen spectroscopic measurement. This is caused by the fact that there are data smaller than the PRad data in the $0.01 \lesssim Q^2 \lesssim 0.05 \text{ GeV}^2$ region, which tend to shift the Δ curve down, increasing the slope and, therefore, the extracted radius. We have also investigated the effect of the PRad data on this fitting. We found that the effect is small, the form factor cut-off slightly increases from 0.8012 ± 0.0010 to $0.8024 \pm 0.0010 \text{ GeV}$ after the inclusion of the PRad data. The small error indicates that the dipole form factor has very small degree of freedom if we include all available data. This is understood since the number of free parameter is only one. As we will see later, this is not the case, when we use different form factors with more free parameters.

3.2. *Fitting to Higher Q^2 Data*

Having shown that the higher Q^2 data may significantly influence the result of extracting the proton charge radius at the $Q^2 \approx 0$ region, we are in the position to investigate the effect of higher Q^2 data to this end. As stated in Sec. 2, there is a visible structure at $Q^2 \approx 0.2 \text{ GeV}^2$ which forces us to introduce some physics to account this phenomenon. Obviously, the use of dipole form factor is inadequate to fit this structure. An alternative solution has been proposed by Friedrich and Walcher.¹⁴

A list of references to the available experimental data is given in Table 1. From this Table it is apparent that the high Q^2 data originate from relatively older experiments. The newest experiments are racing to reach the lowest possible Q^2 region.

The results of fitting free parameters of the dipole, double-dipole, Friedrich-Walcher, and Arrington form factors are given in Tables 2, 3, 4, and 5, respectively. From these Tables it is obvious that the new data deviate significantly from the standard dipole parameterization. The dipole parameterization can give a better agreement with data, but it is also clear that the double-dipole form factor yields a much better agreement due to the larger number of free parameters. This is also true for the Friedrich-Walcher and Arrington form factors, except in these form factors more physics is involved. Nevertheless, due to the large data errors in the large Q^2 region, the smaller χ^2 does not directly show the best parameterization, especially when we discuss the structure at $Q^2 \approx 0.2 \text{ GeV}^2$.

A quick glance at Tables 2-5 reveals that the extracted radii from all refitted models are smaller than the values obtained from the conventional elastic electron-proton scattering. This result is corroborated by our result in the previous discussion on the new PRad data and shown in Fig. 3. However, we will discuss this later, when we compare our present result with those given by previous works in Fig. 6, because it is easier to analyze them by using this figure.

For the electric form factor $G_{E,p}$, comparisons between the fitted models and experimental data are shown in Fig. 4, where we display the electric form factor $G_{E,p}$, the electric form factor in the unit of the standard dipole one $G_{E,p}/G_{SD}$, and the difference between the electric and the standard dipole form factors $G_{E,p} - G_{SD}$,

Table 1. Experimental data used in the present analysis along with their references and corresponding virtual photon momentum squared (Q^2) ranges.

Form Factor	Q^2 Range (GeV ²)	Reference
$G_{E,p}$	0.78 - 1.75	Albrecht <i>et al.</i> ³²
	1.75 - 8.83	Andivahis <i>et al.</i> ³³
	0.39 - 4.095	Bartel <i>et al.</i> ³⁴
	0.39 - 4.09	Behrend <i>et al.</i> ³⁵
	0.39 - 1.95	Berger <i>et al.</i> ³⁶
	0.975 - 1.755	Berkelman <i>et al.</i> ³⁷
	0.0152 - 0.5524	Bernauer <i>et al.</i> ³⁸
	0.00136 - 0.123	Borkowski <i>et al.</i> ³⁹
	0.389 - 1.752	Chen <i>et al.</i> ⁴⁰
	0.65 - 5.2	Christy <i>et al.</i> ⁴¹
	0.273 - 1.755	Hanson <i>et al.</i> ⁴²
	0.0058 - 5.2	Hohler <i>et al.</i> ⁴³
	0.156 - 0.858	Janssens <i>et al.</i> ⁴⁴
	0.00585 - 0.3097	Murphy <i>et al.</i> ⁴⁵
	0.0389 - 1.75	Price <i>et al.</i> ⁴⁶
	0.00546 - 0.0546	Simon <i>et al.</i> ⁴⁷
	0.15 - 9.7	Walker <i>et al.</i> ⁴⁸
	0.00134 - 0.0154	Weber <i>et al.</i> ⁴⁹
	0.000215 - 0.01547	Xiong <i>et al.</i> ⁵⁰
0.0007 - 0.05819	Xiong <i>et al.</i> ⁵⁰	
$G_{M,p}/\mu_p$	0.78 - 1.75	Albrecht <i>et al.</i> ³²
	1.75 - 8.83	Andivahis <i>et al.</i> ³³
	2.883 - 31.28	Arnold <i>et al.</i> ⁵¹
	0.39 - 4.095	Bartel <i>et al.</i> ³⁴
	0.67 - 3.0	Bartel <i>et al.</i> ⁵²
	0.39 - 4.28	Behrend <i>et al.</i> ³⁵
	0.39 - 1.95	Berger <i>et al.</i> ³⁶
	0.975 - 1.755	Berkelman <i>et al.</i> ³⁷
	0.0152 - 0.5524	Bernauer <i>et al.</i> ³⁸
	0.021 - 0.123	Borkowski <i>et al.</i> ³⁹
	0.49 - 1.75	Bosted <i>et al.</i> ⁵³
	0.389 - 3.89	Chen <i>et al.</i> ⁴⁰
	0.65 - 5.2	Christy <i>et al.</i> ⁴¹
	0.669 - 25.03	Coward <i>et al.</i> ⁵⁴
	0.273 - 1.755	Hanson <i>et al.</i> ⁴²
	0.017 - 5.2	Hohler <i>et al.</i> ⁴³
	0.156 - 1.17	Janssens <i>et al.</i> ⁴⁴
	0.999 - 25.03	Kirk <i>et al.</i> ⁵⁵
	1.858 - 15.754	Longwu Ou <i>et al.</i> ⁵⁶
	0.0389 - 3.0	Price <i>et al.</i> ⁴⁶
2.862 - 31.2	Sill <i>et al.</i> ⁵⁷	
0.15 - 9.7	Walker <i>et al.</i> ⁴⁸	

as functions of Q^2 . These three methods of presenting the proton electric form factor are intended to look for the best and sensitive way to compare the performance of different parameterizations.

From panel (a) of Fig. 4 we can see that the plot of $G_{E,p}$ cannot clearly distin-

Table 2. Cut-off parameter of the standard dipole form factor used in the present analysis and that of the dipole form factor extracted from all existing data up to 10 GeV. Note that $N_{\text{dof}} = N_{\text{data}} - N_{\text{par}}$, with N_{dof} , N_{data} , and N_{par} are numbers of degrees of freedom, data, and parameters, respectively.

Parameter	Standard Dipole	Dipole
Λ (GeV)	0.8426	0.8145 ± 0.0003
r (fm)	0.8109	0.8388 ± 0.0003
χ^2	12031	1312
N_{data}	357	357
χ^2/N_{dof}	33.701	3.675

Table 3. As in Table 2, but for the double dipole form factor.

Parameter	Extracted from data
a_0	0.9803 ± 0.0023
a_1 (GeV ²)	0.6932 ± 0.0023
a_2 (GeV ²)	0.0925 ± 0.0117
r (fm)	0.8714 ± 0.0093
χ^2	702
N_{data}	357
χ^2/N_{dof}	1.9674

Table 4. As in Table 2, but for the Friedrich-Walcher form factor.¹⁴

Parameter	Extracted from data	Original values
a_0	1.0031 ± 0.0016	1.041 ± 0.040
a_1 (GeV ²)	0.6774 ± 0.0020	0.765 ± 0.066
a_2 (GeV ²)	6.50 ± 4.43	6.2 ± 5.0
a_b (GeV ⁻²)	-0.1227 ± 0.0068	-0.23 ± 0.18
Q_b (GeV)	0.1969 ± 0.0085	0.07 ± 0.88
σ_b (GeV)	0.1001 ± 0.0811	0.27 ± 0.29
r (fm)	0.8362 ± 0.0110	0.7976 ± 0.0304
χ^2	608	59.71
N_{data}	357	64
χ^2/N_{dof}	1.703	0.933

guish the difference between the 7 parameterizations discussed above. Only at very high Q^2 the difference among them shows up. Unfortunately, the presently available data cannot single out the best parameterization from our calculation. Moreover, the structure at $Q^2 \approx 0.2$ GeV² cannot be seen here.

The electric form factor in the unit of the standard dipole one $G_{E,p}/G_{\text{SD}}$ shown in panel (b) of Fig. 4 starts to display the difference between the parameterizations at $Q^2 \gtrsim 0.2$ GeV². However, since the interesting structure is shown by the data at $Q^2 \approx 0.2$ GeV², the plot of $G_{E,p}/G_{\text{SD}}$ does not help too much in this case. Furthermore, as shown in this panel, relative to the standard dipole one, most of

Table 5. As in Table 2, but for the Arrington form factor.⁵ Note that the parameter error bars in the original values of Arrington model were not reported in their paper.⁵

Parameter	Extracted from data	Original values
a_1	-2.4028 ± 0.0580	3.439
a_2	19.721 ± 0.7835	-1.602
a_3	29.998 ± 20.917	0.068
b_1	8.8857 ± 0.0630	15.055
b_2	-4.9173 ± 4.4649	48.061
b_3	469.26 ± 15.661	99.304
b_4	-530.54 ± 72.354	0.012
b_5	2807.5 ± 125.49	8.650
r (fm)	0.8650 ± 0.0003	0.8774
χ^2	607	43.12
N_{data}	357	56
χ^2/N_{dof}	1.699	0.77

the parameterizations quickly decrease as the Q^2 increases from 1 GeV². Therefore, comparison between data and models is less useful for the present purpose.

Only the third method, which uses $\Delta \equiv G_{E,p} - G_{\text{SD}}$ shown in panel (c), gives the clearest information for our present purpose, since the structure around 0.2 GeV² is clearly revealed by experimental data and model calculations. Interestingly, panel (c) of Fig. 4 also indicates that the proton electric form factor $G_{E,p}$ is approaching the standard dipole one G_{SD} not only at low Q^2 , but also at high Q^2 region, although in the latter experimental data are wildly scattered with large error bars. The fact that all form factors approaches the standard dipole one does not appear in panel (b) since all form factors decrease faster than the standard dipole one. However, since at high Q^2 all form factors are very tiny and inaccessible through experiment, we may conclude that the third method is the best one to compare all form factor models. From panel (c) of Fig. 4 it is clear that the structures near 0.2 GeV² and the differences between the presented models could be investigated if we had experimental data with comparable accuracies to those at low Q^2 .

To investigate the structure near $Q^2 = 0.2$ GeV² let us focus our attention on panel (c) of Fig. 4, especially in the range of $0.001 \lesssim Q^2 \lesssim 10$ GeV². This is shown in Fig. 5, where we compare the analyzed models with experimental data. By looking at the data in the range of $0.05 \lesssim Q^2 \lesssim 5$ GeV² we can infer that there are at least two minima located at $Q^2 \approx 0.1$ and 0.2 GeV². Another possible minimum is seen at $Q^2 \approx 0.4$ GeV², which is less visible than the previous two. Clearly, these minima cannot be produced by the dipole form factor, since as shown in Fig. 5, this form factor can only create one minimum, due to its smooth behavior. The same phenomenon is also displayed by the double dipole one.

As stated by Friedrich and Walcher,¹⁴ the structure can be best described by using the non-smooth term G_{ns} given by Eq. (15). As shown in Fig. 5, by using this term, the original F-W model is able to produce two minima at $Q^2 \approx 0.15$ and 2

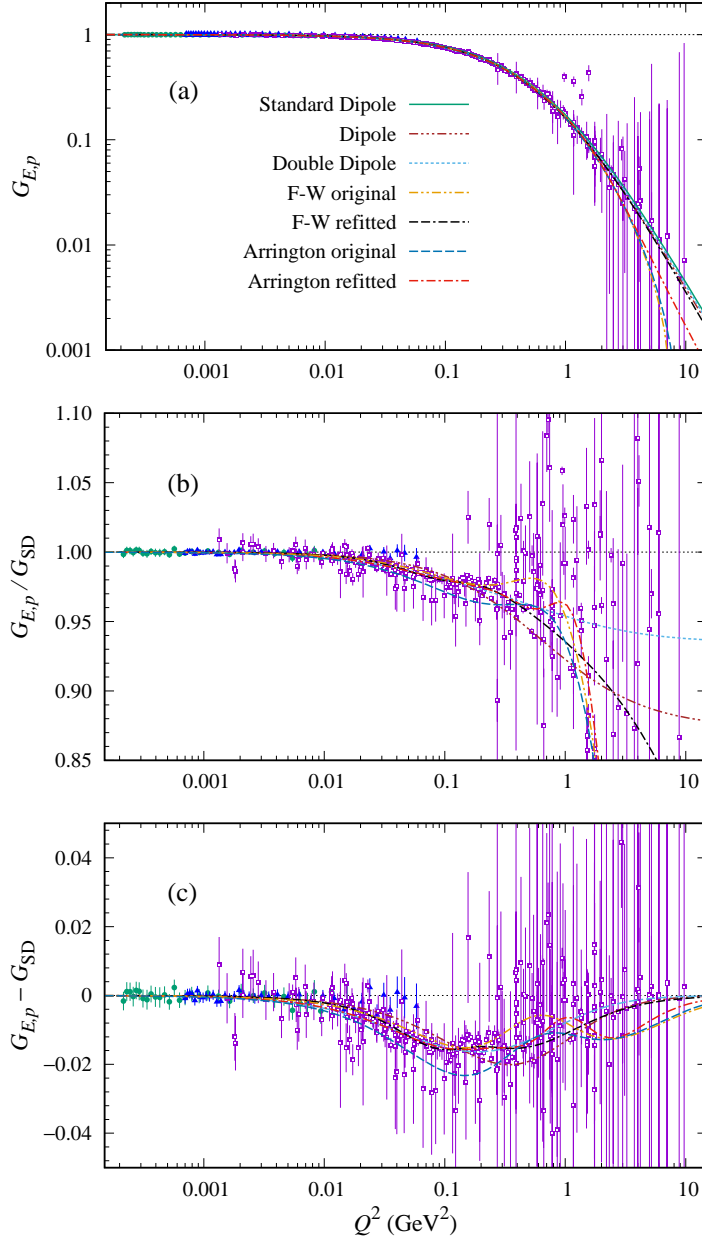


Fig. 4. The proton electric form factor $G_{E,p}$ obtained from the present and previous works compared with experimental data. The form factor is displayed in three different forms, i.e., (a) the original one $G_{E,p}$, (b) divided by the standard dipole one $G_{E,p}/G_{SD}$, and (c) subtracted from the standard dipole one $G_{E,p} - G_{SD}$. The models of Friedrich-Walcher (F-W) and Arrington are obtained from Refs.¹⁴ and.⁵ See Table 1 for the references of the experimental data. The new experimental data from the PRad collaboration *et al.*⁶ are shown in solid green circles (obtained with $E_e = 1.1$ GeV) and solid blue triangles (obtained with $E_e = 2.2$ GeV).

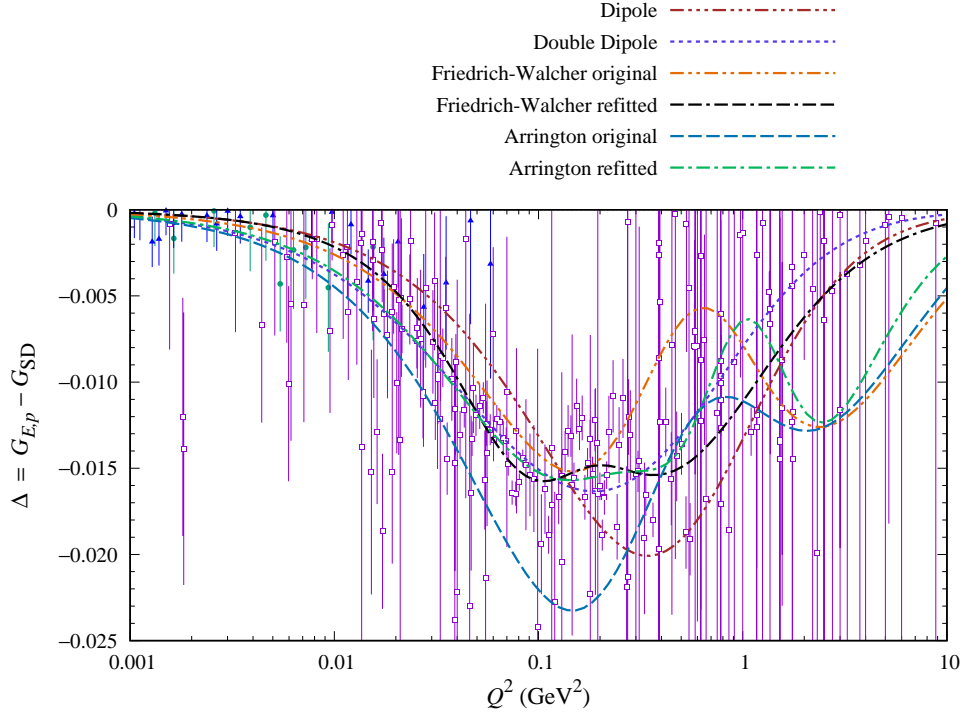


Fig. 5. As in panel (c) of Fig. 4, but zoomed at the structure near $Q^2 = 0.2 \text{ GeV}^2$.

GeV^2 . The refitted F-W model shifts these two minima closer to experimental data, i.e., at $Q^2 \approx 0.1$ and 0.3 GeV^2 .

The original Arrington model also produces two minima with their positions very close to those of the original F-W one. The two models differ only in their form factor magnitudes. As in the case of refitted F-W model, the refitted Arrington model is much closer to experimental data. The remarkable difference here is that the refitted Arrington model produces three minima at $Q^2 \approx 0.1, 0.3$ and 2 GeV^2 . It is of course somewhat strange that both original F-W and Arrington models have a minimum at 2 GeV^2 , whereas almost no experimental data support this phenomenon. Even the refitted Arrington model has also a minimum at this position. Presumably, it is the way of the models to produce a peak at 0.8 GeV^2 , where a number of experimental data points are located.

From Fig. 5 we observe that for $Q^2 \rightarrow 0$ the softest slope (relative to the horizontal $\Delta = 0$ line) is obtained for the Dipole and refitted F-W models, whereas the steepest one is given by the original Arrington model. From this observation, we can estimate that the smallest radius is obtained by the Dipole and refitted F-W models, while the largest radius is obtained by the original Arrington model.

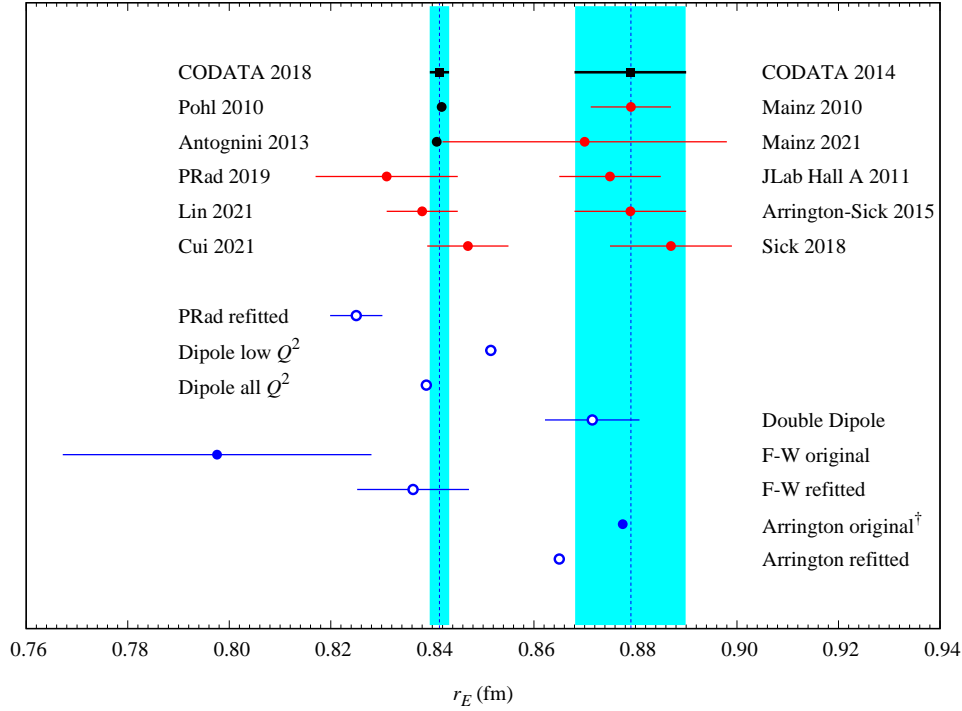


Fig. 6. The extracted proton electric rms radius $r_E \equiv \sqrt{\langle r_{E,p}^2 \rangle}$ obtained in the present and previous works compared with the recommended values of the CODATA-2014³⁰ and CODATA-2018.³¹ The previous works are Pohl 2010,⁸ Mainz 2010,² Antognini 2013,⁶⁷ Mainz 2021,⁴ PRad 2019,⁶ JLab Hall A 2011,⁶² Lin 2021,⁶³ Arrington-Sick 2015,⁶⁴ Cui 2021,⁶⁵ and Sick 2018.⁶⁶ The previous works obtained from analyses of ep scattering data are marked with red circles, whereas those obtained from muonic hydrogen atom are marked with solid black ones. All results obtained from present work are shown by using open circles. Note that the original Arrington model did not report error bars.

This is proven in Fig. 6 and will be discussed later. At this stage it is important to emphasize that the different slopes obtained from different models shown in Fig. 5 are strongly related to different descriptions of the structure near $Q^2 \approx 0.2 \text{ GeV}^2$. In other words, the experimental data at this kinematics significantly influence the calculated proton radius. Therefore, our present work recommends that future experiments should focus on this kinematics instead of going to lower Q^2 . We note that similar conclusion can be also found in previous works.^{58–60} By comparing the models shown in Fig. 5, we believe that experimental data with the same accuracy as the latest data from JLab, for instance, would significantly help to clarify whether the three minima really exist and, therefore, to single out the best parameterization that globally fits the form factor data from 0.0001 to 10 GeV^2 .

Now, let us consider the extracted proton radius from the different models that

we have discussed above. The result is shown in Fig. 6 by the open circles. There are many analyses of this radius in the literature and, as a consequence, only recent results are displayed in Fig. 6.

A newer radius obtained by using initial state radiation (ISR) in MAMI Mainz and formally published in 2021 is smaller than the Mainz 2010 result. However, the quoted error is significantly large, making it consistent with both values obtained from the conventional elastic electron-proton scattering experiments and muonic hydrogen spectroscopic measurement. On the other hand, instead of measuring the cross section, the JLab Hall A experiment⁶² utilized the polarization transfer of electron-proton elastic scattering in the region of $Q^2 = 0.3 - 0.7 \text{ GeV}^2$ and obtained the radius which is consistent with the value obtained from the Mainz-2010 electron-proton scattering experiment.²

More recently, the PRad collaboration performed an experiment at JLab and succeeded to reach much lower Q^2 by using a new electromagnetic calorimeter that could cover a larger area, with a hole in the center to allow the non-scattered electrons to pass through, and therefore could reach much smaller scattering angles.⁶ It is widely known that the problem to reach smaller Q^2 is related to the problem of dealing with very forward scattering angles. The result of this experiment is more precise than that of the polarization transfer experiment at Hall A. As shown in Fig. 6, a smaller radius consistent with the value from muonic hydrogen spectroscopic measurement⁸ was obtained. As discussed in the previous Section we have refitted the PRad data by means of a dipole form factor and obtained a consistent result as shown in the same figure. The smaller error obtained in this case originates from the nature of dipole form factor, which has only one parameter and, as a consequence, a very simple error formula given by Eq. (11), where $\Delta\Lambda$ is obtained from MINUIT. This phenomenon was also found in our previous study.⁶⁹⁻⁷²

The next interesting result is shown by four theoretical calculations, with two of them consistent with the muonic hydrogen value, whereas the other two consistent with the value from electron-proton scattering experiment. By using an improved two-pion continuum, Lin *et al.* found smaller radius⁶³ consistent with the muonic hydrogen value. A similar result was obtained by Cui *et al.*, who analyzed the PRad data by means of a statistical sampling approach. Different result was obtained by Arrington and Sick.⁶⁴ By using a global fit to elastic electron-proton data they obtained a radius of $0.879 \pm 0.011 \text{ fm}$, which is identical to the CODATA-2014 value. Sick⁶⁶ continued the investigation by constraining the extrapolation to very low Q^2 region, where no experimental data are available, by using experimental data at finite Q^2 in order to reduce model dependence. He obtained a radius value of $0.887 \pm 0.012 \text{ fm}$, which is consistent with the value from electron-proton scattering experiment too, as shown in Fig. 6.

It is interesting to see that our fits (indicated by open circles in Fig. 6) using dipole form factor to both low Q^2 and all Q^2 data are mostly closer to the value obtained from the muonic hydrogen atom spectroscopy. The relatively large difference obtained from fit to PRad and fit to all low Q^2 data is a clear indication of the

difference between the two data sets, as has been stated in the previous section. It is also interesting that, by using all data, including the highest Q^2 ones, the extracted radius decreases and approaches the muonic hydrogen atom value. This is the clear evidence that the high Q^2 data have significant effect on the extracted radius. As a consequence, high Q^2 data could become a stringent constraint to the existing models that try to extract the proton charge radius.

Surprisingly, fitting to all data but with a double dipole form factor results in a larger radius, consistent with the value obtained from the conventional electron-proton scattering experiment. Once again, this result indicates that the extraction of radius also depends strongly on the form factor model. Compared to the dipole form factor, the larger error in this case originates from the larger number of degrees of freedom (free parameters). However, if we look back to Fig. 5, we observe that the double dipole form factor yields only one minimum at $Q^2 \approx 0.2 \text{ GeV}^2$ and, therefore, does not precisely reproduce the structure shown by experimental data at this kinematics.

As previously discussed, the more precise models that reproduce the structure around $Q^2 \approx 0.2 \text{ GeV}^2$ are the F-W and Arrington models. Original calculations of these models yield also different radii. Whereas the original F-W model predicted a smaller radius than the muonic hydrogen atom one, the Arrington model corroborates the conventional electron-proton scattering radius.

Interestingly, refitting the two models to new data shifts their radii closer to each other, i.e., increases the F-W radius and decreases the Arrington one. The origin of this phenomenon can be traced back to Fig. 5. Refitting the F-W model shifts the second minimum to a lower Q^2 , where more experimental data show a minimum. This process makes the corresponding slope to the $Q^2 = 0$ point steeper and, as a consequence, makes the extracted radius larger. In the case of Arrington model, the refitting process increases the number of minima from two to three. This is possible since, as shown in Eq. (20), the Arrington model has more complex functions of Q^2 . In this case, the new minimum is located at $Q^2 \approx 0.4 \text{ GeV}^2$. This new minimum makes the slope of form factor, relative to the standard dipole one, softer and, therefore, makes the extracted radius smaller.

Note that as shown in Tables 4 and 5, the difference between the χ^2 's obtained from F-W and Arrington models is almost negligible (608 and 607). However, by carefully looking at Fig. 5, we believe that the F-W model is closer to reproduce experimental data at two minima near 0.1 and 0.4 GeV^2 , whereas the third minimum of Arrington model near 2 GeV^2 seems to be unsupported by experimental data. Therefore, our present study prefers the refitted Friedrich-Walcher model that yields a radius of $0.836 \pm 0.011 \text{ fm}$, consistent with the muonic hydrogen atom value. Nevertheless, a more quantitative conclusion should wait for more precise experimental data in this kinematical region. As stated before, experimental data with accuracy comparable to the latest data in the low Q^2 region would be very decisive to this end.

To emphasize the importance of including higher Q^2 data in the extraction of

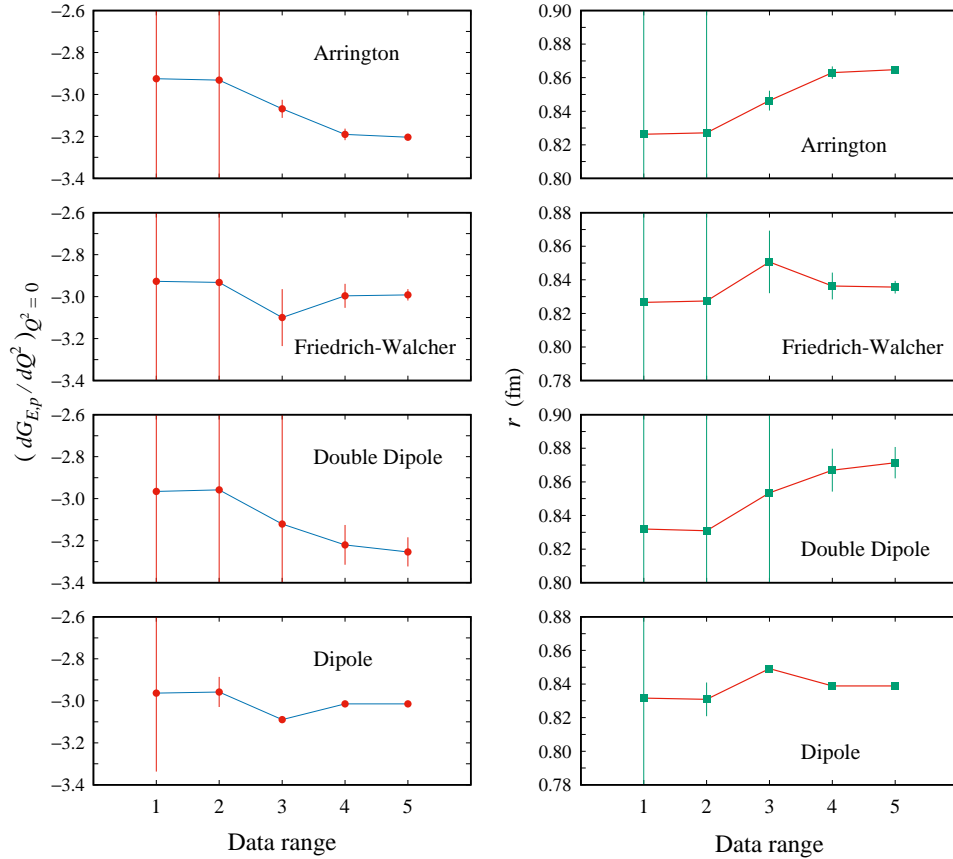


Fig. 7. Derivatives of the proton electric form factor calculated at photon point $|dG_{E,p}/dQ^2|_{Q^2=0}$ (left panels) and the corresponding proton charge radii (right panels) as functions of the data range used in the fitting database for different types of form factor indicated in each panel. The data ranges are (1) $0 < Q^2 < 10^{-3}$, (2) $0 < Q^2 < 10^{-2}$, (3) $0 < Q^2 < 10^{-1}$, (4) $0 < Q^2 < 1$, and (5) $0 < Q^2 < 10 \text{ GeV}^2$.

proton charge radius, in Fig. 7 we show the effect of the data range used in the fit on the extracted form factor derivatives at photon point along with the corresponding proton charge radii. For this purpose we divide the available data into five data ranges written in detail in the caption of Fig. 7.

From the data shown in Fig. 4(c) we would expect that the largest effect could be obtained if we included the data near the structure, i.e., with Q^2 between 0.01 and 1 GeV^2 , which corresponds to the use of the data ranges 3 and 4. This is proven by both the form factor derivatives at photon point and the corresponding proton charge radii shown in Fig. 7. All form factors show significant derivative or radius changes once we switch from the data range 2 to 3, as well as from the data range

3 to 4. Furthermore, as expected from the data shown in Fig. 4(c), the use of data range 1 or 2 does not produce different derivatives or radii. The same phenomenon is also observed in the case of data range 4 or 5. This result emphasizes our previous finding that the inclusion of data with Q^2 between 0.01 and 1 GeV² significantly changes the form factor slope to the $Q^2 = 0$ point, as discussed above.

The large error bars obtained from fitting the data range 1 or 2, especially in the case of Arrington and Friedrich-Walcher form factors, originate from the number of used free parameters, which is unnecessarily too large to fit the relatively few data points. This is not the case for the dipole form factor, since it has only one free parameter. To conclude this section, we have shown that the use of higher Q^2 data has a significant effect on the extracted proton charge radius.

3.3. *The magnetic radius of proton*

For completeness, in Fig. 8 we also present the proton magnetic form factor $G_{M,p}/\mu$, where we display the behavior of the form factor in the form of $G_{M,p}/\mu G_{SD}$ and $G_{M,p}/\mu - G_{SD}$, similar to the case of electric form factor discussed above. It is important to note here that the ratio $G_{M,p}/\mu G_{SD}$ reveals the second structure (peak or maximum) clearly at $Q^2 \approx 2$ GeV² while the difference $G_{M,p}/\mu - G_{SD}$ display both structures at $Q^2 \approx 0.2$ and 1-2 GeV² moderately.

Different from the electric form factor, here we see that the refitted F-W and Arrington models agree with each other, while the difference between the original models is more obvious in panel (c) of Fig. 8, since the difference only exists in the first structure (minimum) at 0.2 GeV².

The extracted proton magnetic radii r_M obtained in the present work are shown in Fig. 9 by open circles, along with those previously calculated and available in literature. In this figure we compare the radii with that of the Particle Data Group⁶⁸ (PDG), i.e., $r_M = 0.851 \pm 0.026$ fm. Here we can see that most of the calculations agree with the PDG estimate. This is very different from the case of charge radius. The proton magnetic radii extracted from refitting the F-W and Arrington models are also moving closer to each other, as expected from the behavior of their form factors for small Q^2 shown in Fig. 8. While the refitted F-W model yields $r_M = 0.821 \pm 0.004$ fm, the Arrington refitted one yields $r_M = 0.826 \pm 0.002$ fm. Thus, the extracted radii from the two models are consistent to each other as well as to the PDG estimate. The present calculation indicates that refitting models with the new data from very low to very high Q^2 can improve the agreement of the extracted proton magnetic radii.

4. Summary and Conclusion

We have revisited the extraction of proton electric and magnetic radii. To this end we presented a number of form factor models commonly used to extract the radii. The formulation of the models along with the corresponding error were also derived. Special attention was given to the higher Q^2 region, where two structures

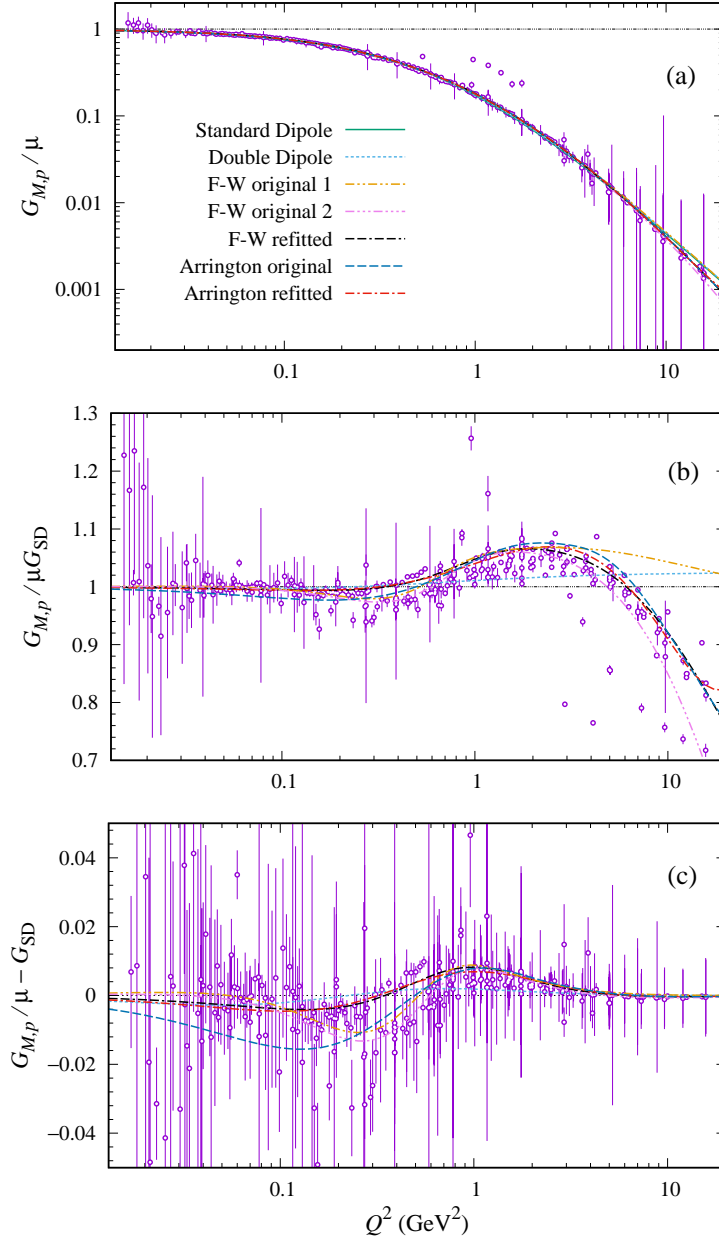


Fig. 8. The proton magnetic form factor $G_{M,p}/\mu$ obtained from the present and previous works compared with experimental data. The form factor is displayed in three different forms, i.e., (a) the original one $G_{M,p}/\mu$, (b) divided by the standard dipole one $G_{M,p}/\mu G_{SD}$, and (c) subtracted from the standard dipole one $G_{M,p}/\mu - G_{SD}$, with μ the proton magnetic moment in the unit of nuclear magneton. As in Fig. 4 the models of Friedrich-Walcher (F-W) and Arrington are obtained from Refs.¹⁴ and ⁵.

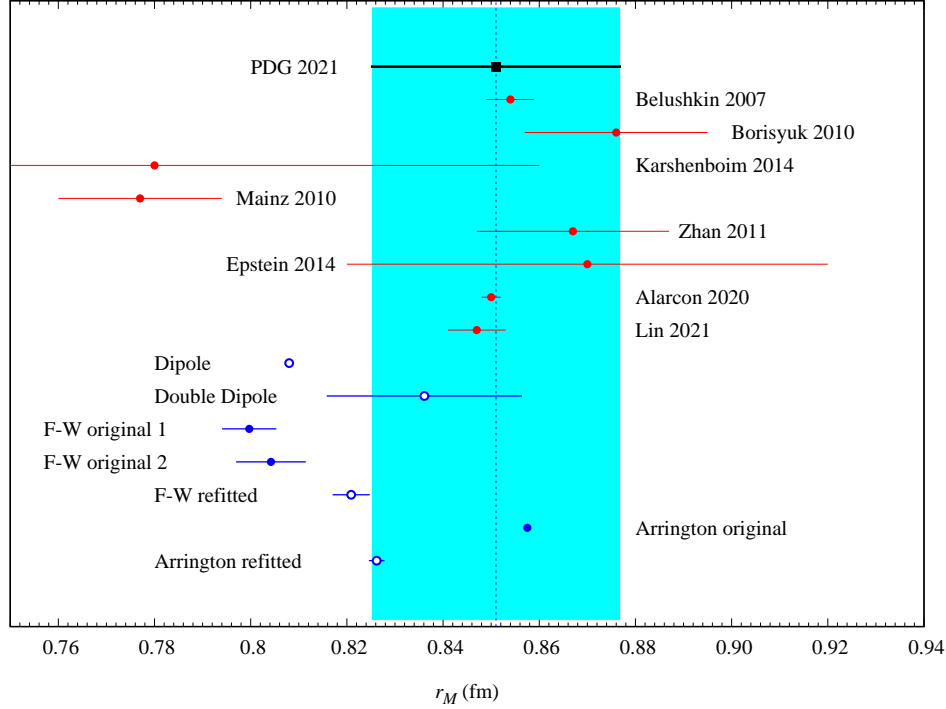


Fig. 9. As in Fig. 6 but for the proton magnetic radius $r_M \equiv \sqrt{\langle r_{M,p}^2 \rangle}$ obtained from the present and previous works compared with the recommended value obtained from PDG 2021.⁶⁸ The previous works are obtained from theoretical works of Belushkin 2007,⁷³ Borisuyuk 2010,⁷⁴ Zhan 2011,⁶² Karshenboim 2014,⁷⁵ Epstein 2014,⁷⁶ Alarcon 2020,²⁵ Lin 2021,⁶³ and experimental work from Mainz 2010.⁶¹ As in Fig. 6, the radius error bar of the Arrington original model was not reported.

are exhibited by experimental data. To this end we exploited two form factor models that were previously used to globally fit the data, i.e., the Friedrich-Walcher and Arrington parameterizations, along with the dipole and double-dipole ones. Since the new PRad data at very low Q^2 gave surprisingly small charge radius, consistent with the value from muonic hydrogen spectroscopic measurement, but in contrast to the previous experiments using elastic electron-proton scattering, we first reanalyzed the data by using a simple dipole form factor. We extracted the radius and obtain a relatively small value, consistent with the PRad's reported value, although we used different form factor. By including the higher Q^2 data we observed at least two structures (minima) at $Q^2 \approx 0.1$ and 0.2 GeV². The dipole and double dipole form factors produced only one minimum. The refitted Friedrich-Walcher and Arrington form factors could nicely reproduce these structures, but the Friedrich-Walcher one seems to be the more natural. The latter yielded a radius of 0.836 ± 0.011 fm, which

is consistent to the radius obtained from muonic hydrogen atom. We have also reanalyzed the magnetic form factor data and obtained the magnetic radii consistent with the PDG 2021 estimate if we used the Friedrich-Walcher and Arrington form factors. Although our analysis indicates that the higher Q^2 data play a significant role in extracting the proton electromagnetic radii, a more definite conclusion could be drawn only after we have new data at this kinematics with error comparable to the present experiments.

Acknowledgment

This work was supported by a special grant provided by Universitas Indonesia under contract No. NKB-587/UN2.RST/HKP.05.00/2021.

References

1. R. Hofstadter and R. W. McAllister, Phys. Rev. **98**, 217 (1955).
2. J. Bernauer *et al.*, Phys. Rev. Lett. **105**, 242001 (2010).
3. M. Mihovilović *et al.*, Phys. Lett. B **771**, 194 (2017).
4. M. Mihovilović *et al.*, Eur. Phys. J. A **57**, 107 (2021).
5. J. Arrington, W. Melnitchouk and J. A. Tjon, Phys. Rev. C **76**, 035205 (2007).
6. W. Xiong *et al.*, Nature **575**, 147 (2019).
7. G. A. Miller, Phys. Rev. C **99**, 035202 (2019).
8. R. Pohl *et al.*, Nature, **466** 213 (2010).
9. A. Beyer *et al.*, Science **358**, 79 (2017).
10. H. Fleurbaey *et al.*, Phys. Rev. Lett. **120**, 183001 (2018).
11. N. Bezginov, T. Valdez, M. Horbatsch, A. Marsman, A. C. Vutha, and E. A. Hessels, Science **365**, 1007 (2019).
12. A. Grinin, A. Matveev, D. C. Yost, L. Maisenbacher, V. Wirthl, R. Pohl, T. W. Hänsch, and T. Udem, Science **370**, 1061 (2020).
13. H. Gao and M. Vanderhaeghen, Rev. Mod. Phys. **94**, 015002 (2022).
14. J. Friedrich and Th. Walcher, Eur. Phys. J. A **17**, 607 (2003).
15. H. Atac, M. Constantinou, Z.-E. Meziani, M. Paolone, and N. Sparveris, Eur. Phys. J. A **57**, 65 (2021).
16. J. Arrington, J. Phys. Chem. Ref. Data **44**, 031203 (2015).
17. F. Hagelstein and V. Pascalutsa, Phys. Lett. B **797**, 134825 (2019).
18. M. Horbatsch and E. A. Hessels, Phys. Rev. C **93**, 015204 (2016).
19. K. Griffioen, C. Carlson and S. Maddox, Phys. Rev. C **93**, 065207 (2016).
20. D. W. Higinbotham, A. A. Kabir, V. Lin, D. Meekins, B. Norum and B. Sawatzky, Phys. Rev. C **93**, 055207 (2016).
21. M. O. Distler, T. Walcher and J. C. Bernauer, [arXiv:1511.00479 [nucl-ex]].
22. X. Yan, D. W. Higinbotham, D. Dutta, H. Gao, A. Gasparian, M. A. Khandaker, N. Liyanage, E. Pasyuk, C. Peng and W. Xiong, Phys. Rev. C **98**, 025204 (2018).
23. J. M. Alarcón, D. W. Higinbotham, C. Weiss and Z. Ye, Phys. Rev. C **99**, 044303 (2019).
24. S. K. Barcus, D. W. Higinbotham and R. E. McClellan, Phys. Rev. C **102**, 015205 (2020).
25. J. M. Alarcón, D. W. Higinbotham and C. Weiss, Phys. Rev. C **102**, 035203 (2020).
26. G. Paz, Mod. Phys. Lett. A **36**, 2150143 (2021)
27. D. Borisjuk and A. Kobushkin, Nucl. Phys. A **1002**, 121998 (2020).

24. M. Ridwan and T. Mart
28. C. Lorcé, Phys. Rev. Lett. **125**, 232002 (2020).
29. F. James and M. Roos, Comput. Phys. Commun. **10**, 343 (1975).
30. P. J. Mohr, D. B. Newell and B. N. Taylor, Rev. Mod. Phys. **88**, 035009 (2016).
31. E. Tiesinga, P. J. Mohr, D. B. Newell and B. N. Taylor, Rev. Mod. Phys. **93**, 025010 (2021).
32. W. Albrecht *et al.*, Phys. Rev. Lett. **17** 1192 (1966).
33. L. Andivahis *et al.*, Phys. Rev. D **50**, 5491 (1994).
34. W. Bartel *et al.*, Phys. Rev. Lett. **17**, 608 (1966).
35. H. J. Behrend *et al.*, DESY Experiment (1966).
36. C. Berger *et al.*, Phys. Lett. B **35**, 87 (1971).
37. K. Berkelman *et al.*, Phys. Rev. **130**, 2061 (1963).
38. J. C. Bernauer, Ph.D. thesis, Johannes Gutenberg-Universität Mainz, 2010.
39. F. Borkowski *et al.*, Z. Phys. A **275**, 29 (1975).
40. K. W. Chen *et al.*, Phys. Rev. **141**, 1267 (1966).
41. M. E. Christy *et al.*, Phys. Rev. C **70**, 015206 (2004).
42. K. M. Hanson *et al.*, Phys. Rev. D **8**, 753 (1973).
43. G. Hohler *et al.*, Nucl. Phys. B **114**, 505 (1976).
44. T. Janssens *et al.*, Phys. Rev. **142**, 922 (1966).
45. J. J. Murphy *et al.*, Phys. Rev. C **9**, 2125 (1974).
46. L. E. Price *et al.*, Phys. Rev. D **4**, 45 (1971).
47. G. G. Simon *et al.*, Nucl. Phys. A **333**, 381 (1980).
48. R. C. Walker *et al.*, Phys. Rev. D **49**, 5671 (1994).
49. A. B. Weber, Ph.D. thesis, Johannes Gutenberg-Universität Mainz, 2017.
50. W. Xiong, Ph.D. thesis, Duke University, 2020.
51. R. G. Arnold *et al.*, Phys. Rev. Lett. **57**, 174 (1986).
52. W. Bartel *et al.*, Nucl. Phys. B **58**, 429 (1973).
53. P. E. Bosted *et al.*, Phys. Rev. C **42**, 38 (1990).
54. D. H. Coward *et al.*, Phys. Rev. Lett. **20**, 292 (1968).
55. P. N. Kirk *et al.*, Phys. Rev. D **8**, 63 (1973).
56. L. W. Ou, Ph.D. thesis, Massachusetts Institute of Technology, 2019.
57. A. F. Sill *et al.*, Phys. Rev. D **48**, 29 (1993).
58. S. Pacetti and E. Tomasi-Gustafsson, Eur. Phys. J. A **56**, 74 (2020).
59. M. Hoballah, S. Cholak, R. Kunne, C. Le Galliard, D. Marchand, G. Quémener, E. Voutier and J. van de Wiele, Eur. Phys. J. A **55**, 112 (2019).
60. S. Pacetti and E. Tomasi-Gustafsson, Eur. Phys. J. A **57**, 72 (2021).
61. J. C. Bernauer *et al.*, Phys. Rev. Lett. **105**, 242001 (2010).
62. X. Zhan *et al.*, Phys. Lett. B **705**, 59 (2011).
63. Y. H. Lin, H. W. Hammer and U. G. Meißner, Phys. Lett. B **816**, 136254 (2021).
64. J. Arrington and I. Sick, J. Phys. Chem. Ref. Data **44**, 031204 (2015).
65. Z. F. Cui, D. Binosi, C. D. Roberts and S. M. Schmidt, Phys. Rev. Lett. **127**, 092001 (2021).
66. I. Sick, Atoms **6**, 2 (2018).
67. A. Antognini *et al.*, Science **339**, 417 (2013).
68. P. A. Zyla *et al.* (Particle Data Group), Prog. Theor. Exp. Phys. 2020, 083C01 (2020) and 2021 update.
69. T. Mart and A. Sulaksono, Phys. Rev. C **87**, 025807 (2013).
70. T. Mart and A. Sulaksono, Phys. Rev. C **88**, 059802 (2013).
71. T. Mart and A. Sulaksono, Phys. Rev. C **93**, 039802 (2016).
72. N. G. Kelkar, T. Mart, and M. Nowakowski, Makara J. Sci. **20**, 119 (2016).
73. M. A. Belushkin, H. W. Hammer and U. G. Meissner, Phys. Rev. C **75**, 035202 (2007).

74. D. Borisjuk, Nucl. Phys. A **843**, 59 (2010).
75. S. G. Karshenboim, Phys. Rev. D **90**, 053013 (2014).
76. Z. Epstein, G. Paz and J. Roy, Phys. Rev. D **90**, 074027 (2014).